Ultradispersed Mo/TiO_2 catalysts for CO_2 hydrogenation to methanol

Thomas Len[a], Mounib Bahri[b], Ovidiu Ersen[b], Yaya Lefkir[c], Luis Cardenas[a], Ignacio Villar[d], Virginia Pérez Dieste[d], Jordi Llorca[e], Noémie Perret[a], Ruben Checa[a], Pavel Afanasiev[a], Franck Morfin[a] and Laurent Piccolo[a*]

[a] Univ Lyon, Université Claude Bernard Lyon 1, CNRS, IRCELYON, F-69626 Villeurbanne, France

[b] Institut de Physique et Chimie des Matériaux de Strasbourg (IPCMS), UMR 7504, CNRS-Université de Strasbourg, 23 rue du Lœss, 67034 Strasbourg Cedex 2, France

[c] Laboratoire Hubert Curien, UMR 5516, 42000 Saint-Etienne, France

[d] ALBA Synchrotron Light Source, Carrer de la Llum 2-26, 08290 Cerdanyola del Vallès, Barcelona, Spain

[e] Institute of Energy Technologies, Department of Chemical Engineering and Barcelona Research Center in Multiscale Science and Engineering, Universitat Politècnica de Catalunya, EEBE, Eduard Maristany 16, 08019 Barcelona, Spain

Abstract

Mo/TiO_2 catalysts with high molybdenum dispersion appear active and stable in the gas-phase hydrogenation of CO_2. The comparison between various titania materials shows a crucial effect of the support nature on the methanol yield. Molybdenum supported on rutile titania nanorods is the most active and methanol-selective system. The catalysts were investigated by aberration-corrected scanning transmission electron microscopy, near-ambient pressure X-ray photoelectron spectroscopy… Monomeric and partially reduced Mo oxo species are suspected to be the active centres.

Introduction

Due to environmental concerns, the reduction of greenhouse gas emissions has become mandatory. In this context, promising approaches for the valorisation of CO_2 have been developed, allowing the synthesis of value-added chemicals such as urea, salicylic acid, cyclic carbonate and polypropylene carbonate at the laboratory scale.[1–3] The most promising valorisation strategy consists in the transformation of effluent CO_2 through catalytic hydrogenation,[4–7] leading to valuable products such as carbon monoxide, hydrocarbons and oxygenates.[8,9] Methanol, a platform chemical with high interest in the production of fuels and plastics,[10,11] is industrially produced from syngas (CO and H_2) in the presence of a $Cu/ZnO/Al_2O_3$ catalyst at 5-10 MPa and 250-300 °C. Researches on CO_2 hydrogenation to methanol have mostly focused on this system, for understanding and optimising its catalytic performances.[12–18] However, this catalyst is pyrophoric, and a serious threat exists in the next decades for zinc availability.[19] Moreover, the generation of water as a by-product of CO_2 hydrogenation induces ZnO agglomeration, Cu oxidation and sintering, leading to catalyst deactivation.[20,21] Hence, it is desirable to find alternative catalysts with enhanced performances.[22–24] This includes not only the catalyst stability but also its activity and selectivity to methanol.[25]

Ultradispersed metal-based catalysts, i.e. single-atom catalysts (SACs) or subnanometric cluster-based catalysts,[26] are an attractive new class of materials which potentially offer maximum atom-efficiency and specific catalytic properties.[27–30] A large fraction of SAC studies has focused on noble metals, with a view to cost reduction. However, the stabilization of single noble-metal atoms on oxides is challenging because of their tendency to aggregation.[26,31–33]

Molybdenum-based catalysts are widely used in petroleum refining, and catalyze syngas conversion to alcohols.[34] Mo has a half-filled d-electron shell and a variable valence state, which makes this oxophillic element suitable for tuning the catalytic performance through coordination engineering.[35] Non-precious catalysts containing Mo-based species supported on TiO_2 (MoO_x/TiO_2, MoS_2/TiO_2, etc.) are well-known for photocatalysis,[36] as well as thermocatalytic oxidation[37,38] and hydrodesulfurization[39–41] reactions. While CO and CO_2 hydrogenation reactions were carried out over Mo/TiO_2,[42–44] this system was found inefficient. Shimizu's group recently reported that the addition of a noble metal such as Pt is mandatory to promote a 30 wt% Mo/TiO_2-P25 sample for the CO_2-to-methanol reaction.[44]

Herein, we disclose the unexpected CO_2 hydrogenation performances of selected low wt% Mo/TiO_2 catalysts. A broad range of TiO_2 materials, Mo loadings and pretreatment conditions were studied to compare their impacts on CO_2 conversion activity and selectivity to methanol.

Experimental section

Catalyst preparation

The TiO_2 samples, the molybdenum precursor (Aldrich, 99.98% trace metals basis) and the reference $Cu/ZnO/Al_2O_3$ catalyst (Thermo Fisher) were used without specific treatment. For titania supports, DT51D (>99.5%) and PC500 (>85%) were purchased from Tronox, P25 and P90 (>99.5%) were purchased from Evonik Aeroxide, and RL11A (>99.5%) was purchased from Solvay.

In a typical preparation, 5 g of TiO_2, an appropriate amount (depending on the target Mo loading) of $Mo_7O_{24}(NH_4)_6.4H_2O$ and 60 mL of deionised water were stirred for 2 h in a round bottom flask. The mixture was dried in a rotary evaporator at 60 °C, and the resulting powder was treated in a flow fixed-bed reactor under H_2 (40 mL/min) for 2 h at 500 °C (5 °C/min).

Catalytic testing

The catalytic tests were performed using a straight stainless-steel flow fixed bed reactor (internal diameter 7 mm), heated with a tubular oven. Gas flows were controlled by Brooks Instruments flowmeters and analysed by an Inficon Fusion micro gas chromatograph equipped with molecular sieve and RT-Q-Bond modules. The temperature program for the RT-Q-Bond was 60 °C for 70 s, then 230 °C for 120 s (2.5 °C/min). The total pressure was set to 30 bar using a Tescom ER5000 electropneumatic PID controller driving a Tescom membrane backpressure regulator. A heating system was set up to keep the temperature above 70 °C in the gas lines in order to avoid condensation. Prior to catalytic tests the as-prepared catalysts were treated *in situ* in the catalytic reactor under H_2 (40 mL/min) for 2 h (5 °C/min) at atmospheric pressure in the 450-700 °C range (standard value 450 °C). The catalytic experiments were conducted with an $H_2/CO_2/N_2$ mixture of 30/10/10 mL/min and 400 mg of catalyst, leading to a gas hourly space velocity (GHSV) of 7500 $mL.g^{-1}.h^{-1}$. The following standard temperature sequence was used for the catalytic tests: from RT to 200 °C at 5 °C/min, then 200 °C to 300 °C at 0.25 °C/min.

Conversion of CO_2 (χ_{CO2}), selectivities to product P (S_P), methanol (MeOH) production turnover frequency (TOF_{MeOH}) and space-time yield (STY_{MeOH}) were calculated as follows, with Q_{CO2}^{in}, Q_i^{out}, n_{Mo}, $M_{MeOH,}$ and m_{cat} representing the flow rate of CO_2 at the reactor inlet, the flow rate of product i at the reactor outlet, the molar amount of Mo, the molar mass of methanol, and the catalyst mass, respectively. For TOF calculations, all Mo atoms were considered as exposed to the gas phase (100% dispersion).

$$\chi_{CO2} = \frac{\sum_i Q_i^{out}}{Q_{CO2}^{in}} \quad S_P = \frac{Q_P^{out}}{\sum_i Q_i^{out}} \quad TOF_{MeOH} = \frac{Q_{CO2}^{in}\,\chi_{CO2}\,S_{MeOH}}{n_{Mo}} \quad STY_{MeOH} = \frac{Q_{CO2}^{in}\,\chi_{CO2}\,S_{MeOH}\,M_{MeOH}\times 1000}{m_{cat}}$$

Catalyst characterisation

Scanning transmission electron microscopy (STEM) with high-angle annular dark field (HAADF) detection was performed on a Jeol Cold FEG NeoARM (point-to-point resolution 0.78 Å, images in Fig. 1) and a Jeol 2100F (point-to-point resolution 1.1 Å, all other images), both equipped with a Cs-corrected condenser at the probe level and operated at 200 kV. For sample preparation, the powder was crushed and dispersed in ethanol through ultrasonication, dropped onto a holey carbon-coated 200 mesh Cu grid, and dried by a lamp. To avoid contamination during analysis and remove any residual carbon, the samples were Ar plasma-cleaned for 20 s (Plasma Prep 5, GaLa Instrumente). No filtering was applied on the STEM images.

NAP-XPS analysis was conducted at the CIRCE beamline at ALBA synchrotron, using a NAPP endstation designed by SPECS GmbH in collaboration with CIRCE beamline. All spectra reported here were acquired combining UHV and H_2/CO_2 environments with the sample held at RT, 200 °C, 275 °C, and 350 °C while the catalyst run at 2 mbar with a 3/1 ratio of H_2/CO_2 mixture. Each sample was previously reduced *in situ* at 400 °C under 2 mbar of H_2. The catalyst in the form of powder was deposited onto an Ag foil previously cleaned to reduce charge effects and for XPS calibration purposes (ref-DOI: 10.1039/C8CP04614J). The spectra are all referenced to the Ag Fermi level, measured after every spectrum, to determine absolute binding energies. A Photon energy of 400 eV was used to probe Mo 3d core-level with high photoionization cross-section under NAP conditions. Sample degradation due to X-ray radiation was not observed. NAP-XPS analysis revealed a well-resolved Mo 3d core level. Each spectrum was decomposed into a combination of Voight functions, each with an overall full-width at half maximum (FWHM) of approximately 1.6 eV.

Hydrogen-assisted temperature programmed reduction (H_2-TPR) was performed using a U-shaped quartz reactor (internal diameter 4 mm). Prior to the TPR, the catalyst (100 mg) was pretreated under He (30 mL/min) at 250 °C (15 °C/min) for 30 min. After return to room temperature, the catalyst was heated at 15 °C/min to 850 °C under 30 mL/min of 1% H_2/He. The outlet gas mixture was analysed by an Omnistar mass spectrometer from Pfeiffer Vacuum. The baseline was subtracted to the resulting H_2 signal, which is quantified using 1% H_2/He as reference value.

CO_2 temperature-programmed desorption (TPD) measurements were conducted on a custom-made apparatus using a U-glass tubular reactor loaded with 100 mg of catalyst. After an *in situ* reduction for 2 h at 450 °C (5 °C/min) under 40 mL/min of H_2, the powder was desorbed at 450 °C under N_2 (100 mL/min) for 4 h. After cooling down to 30 °C, the catalyst was exposed to 5% CO_2 in N_2. Then, the reactor was flushed for 30 min under N_2 before the temperature was increased from 30 °C to 450 °C (5 °C/min) to desorb CO_2. The outlet gases were analysed by infrared spectroscopy and the CO_2 quantity was determined from the asymmetric stretching bands at 2450-2100 cm^{-1} using a calibration curve.

X-ray fluorescence (XRF) analysis was performed using an Epsilon 4 spectrometer from Malvern Panalytical. The generator was used at 50 kV and 60 µA under air atmosphere. Data were collected at the Mo Kα energy level (17.44 keV) using a 3-point calibration curve verified by inductively coupled plasma – optical emission spectroscopy (ICP-OES).

The specific surface areas were determined by N_2 volumetry through a 5-points BET method using a Micrometrics ASAP 2020.

Results and discussion

The catalysts were prepared by conventional wet impregnation followed by a reductive treatment (see Experimental section) The samples, listed in Table 1, are labelled as <*Mo loading in wt%*>Mo/<*TiO_2 material name*>-R<*in situ reduction temperature*>. For example,

3Mo/DT51D-R450 denotes a catalyst containing 3 wt% Mo supported on TiO_2 DT51D (anatase) and reduced *in situ* at 450 °C. XRF measurements (Table 1) show that the Mo loadings were found close to the target values (0.1 to 10 wt%, standard loading 3 wt%) within a relative accuracy of 20%.

Table 1 – Characteristics of the Mo/TiO_2 catalysts used in this study.

Sample name	Specific surface area (m^2/g)[a]	TiO_2 phase composition (anatase/rutile)[b]	Mo loading (wt%)[c]
0.1Mo/DT51D			0.1
0.3Mo/DT51D			0.2
1Mo/DT51D	78	100%/0%	1.0
3Mo/DT51D			2.9
10Mo/DT51D			8.3
3Mo/PC500	148	100%/0%	3.4
3Mo/P90	105	90%/10%	3.3
3Mo/P25	61	80%/20%	2.8
3Mo/RL11A	12	0%/100%	2.6
1Mo/RNR	44	0%/100%	1.0
3Mo/RNR			2.9

[a] Determined by N_2 volumetry through the BET method; [b] Furnisher values, except for RNR: determined from X-ray diffraction; [c] Determined by XRF spectroscopy (standard deviation 0.05 wt%).

Figure 1 displays representative STEM-HAADF micrographs of 3Mo/DT51D and 3Mo/RNR samples. The images suggest that Mo is atomically dispersed at the surface of TiO_2, i.e. it is present as a mixture of single-atoms and subnanometric clusters. The latter correspond to 2D

oxomolybdate clusters, as previously reported in the literature.[38,45–47] STEM micrographs of the other 3 wt% Mo/TiO_2 catalysts (Figure S1) show a similarly high dispersion of Mo. The relative intensities represented in Figures 1C and 1F were determined along the yellow lines in Figure 1B for anatase and 1E for rutile, respectively. Mo atoms are seen to preferentially adsorb at Ti cation positions on both anatase and rutile. This is consistent with previous works on the epitaxial growth of molybdenum nanostructure on titania.[45,46,48–50]

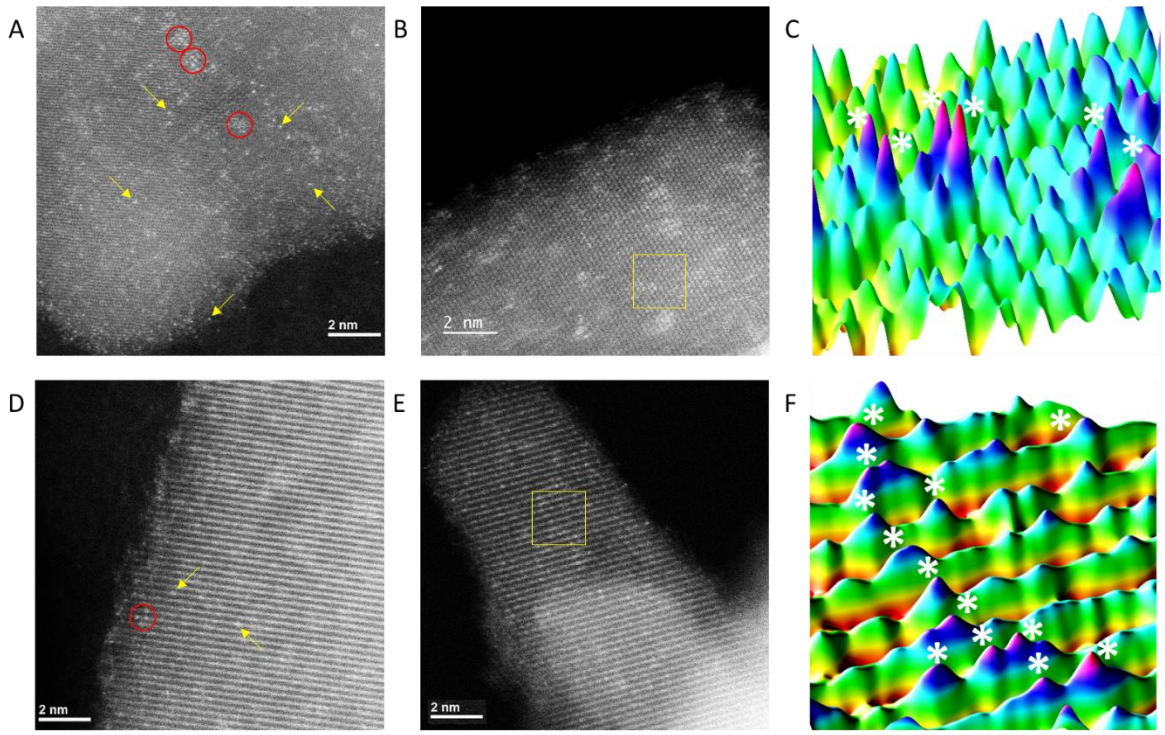

Figure 1 - Representative aberration-corrected STEM-HAADF micrographs. A, B: 3Mo/DT51D; D, E: 3Mo/RNR. Arrows and circles in A and D show single Mo atoms and Mo clusters, respectively. C, F: Intensity representation of the 2 nm^2 yellow square represented in B and E, respectively. The white stars indicate the Mo atoms.

A summary of catalytic properties for the whole set of samples is presented in Table 2. In order to compare the different materials, conversion, selectivity as well as methanol TOF and STY were determined as described in the Experimental section.

Table 2 - CO_2 hydrogenation performances of Mo/TiO_2 samples at 275 °C under 30 bar of $H_2/CO_2/N_2$ (3/1/1), GHSV = 7500 $mL.g^{-1}.h^{-1}$.

Sample	CO_2 conversion (%)	CH_4 selectivity (%)[b]	MeOH selectivity (%)[b]	DME selectivity (%)[b]	MeOH TOF ($mol_{MeOH}.mol_{Mo}^{-1}.h^{-1}$)	MeOH STY ($g_{MeOH}.kg_{cat}^{-1}.h^{-1}$)
0.1Mo/DT51D	0.9	5.2	4.8	4.8	2.81	0.94
0.3Mo/DT51D	3.0	5.9	5.1	2.5	3.20	3.20
0.3Mo/DT51D-R600	1.7	0	4.6	1.7	1.70	1.70
1Mo/DT51D	5.2	12.0	10.2	3.2	3.57	11.31
3Mo/DT51D as prepared	1.7	5.1	23.3	5.9	0.88	8.22
3Mo/DT51D	4.8	8.7	6.6	3.2	0.71	6.84
3Mo/DT51D-R600	10.8	6.1	5.7	1.6	1.33	12.89
3Mo/DT51D-R700	3.8	3.2	15.1	0.7	1.24	12.00
10Mo/DT51D	3.3	9.5	4.9	2.2	0.12	3.41
3Mo/PC500	< 0.1	-	-	-	-	-
3Mo/P90	4.0	10.5	3.7	1.0	0.28	3.09
3Mo/P25	2.6	10.0	5.4	3.1	0.32	3.01
3Mo/RL11A	1.5	4.4	17.8	0	0.57	5.68
1Mo/RNR	7.6	23.1	10.5	1.1	5.16	16.87
3Mo/RNR	6.8	9.3	24.2	1.3	3.61	34.95
50Cu/ZnO/Al_2O_3	20.7	0	32.3	0	0.56	141.06

[a] Samples in situ prereduced at 450 °C except when mentioned otherwise; [b] CO represents the complement to 100%.

From these data, it appears that all the samples except Mo/PC500 are active for CO_2 hydrogenation. The main product is always CO (along with water, which cannot be accurately

quantified), followed by methane or methanol depending on the support oxide, then dimethyl ether (DME). Thus, the main reaction pathway on molybdenum-based catalysts remains CO_2 reduction to CO through the reverse water-gas shit reaction as described by several teams using molybdenum carbide, MoO_x/Ti_3AlC_2 or molybdenum doping Fe/Al_2O_3 and Cu/FAU.[51–55]

Figure 2 allows comparing the titania supports in terms of CO_2 hydrogenation activity and selectivity to methanol at a constant Mo loading of 3 wt%. The CO_2 conversion at 275 °C varies from less than 0.1% for PC500 to 6.8% for RNR. The products distribution also strongly depends on the TiO_2 nature. In particular, the selectivity to methanol ranges from 3.7% for P90 to 24.2% for RNR. As a result, the STY reaches 35 g of methanol per kg of catalyst per hour, versus 141 $g_{MeOH}.kg_{cat}^{-1}.h^{-1}$ for the highly Cu-loaded (50 wt%) industrial $Cu/ZnO/Al_2O_3$ methanol-synthesis catalyst evaluated in the same conditions (Figure S2).

The results of typical experiments at variable temperature are reported in Figure S3 for 3Mo/RNR and 3Mo/DT51D, the two most active systems. CO_2 conversion as well as selectivities to CH_4 and CO increase with the temperature, while the selectivity to methanol decreases. While the 3Mo/RNR catalyst reaches a methanol selectivity of 50% at 200 °C, a climax of 23 % is obtained at 220 °C on 3Mo/DT51D, with CO as the main by-product for the two catalysts. These two catalysts exhibit stable catalytic performance for 40 h (Figure S4).

Notably, these performances correlate neither with the specific surface area of TiO_2 (Figure S5), nor with the titania phase composition as anatase-pure DT51D and rutile-pure RNR are the supports that promote the highest activities.

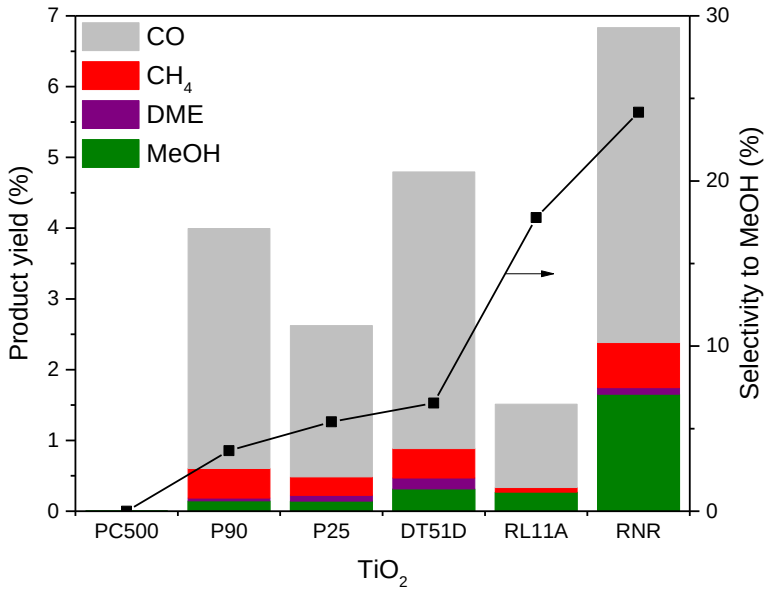

Figure 2 - Effect of TiO_2 nature on product yields and methanol selectivity for 3Mo/TiO_2 catalysts at 275 °C under 30 bar of $H_2/CO_2/N_2$ (3/1/1), GHSV = 7500 mL.g^{-1}.h^{-1}.

Synchrotron-based NAP-XPS was performed to tentatively clarify the atomic origins of the support-dependent performances in terms of Mo oxidation state. The experiments were carried out on 3Mo/RNR, 3Mo/P25, and 3Mo/DT51D under conditions of *in situ* reduction (H_2, 400 °C) and reaction (75 vol% H_2 + 25 vol% CO_2, 200-350 °C) at 2 mbar total pressure. Figure 3a shows Mo 3d core-level spectra recorded of 3Mo/DT51D and 3Mo/RNR samples under H_2-CO_2 mixture at 275 °C. The XPS results obtained for all the samples and conditions are presented in Figure S6 and Table S1, and synthetized in Figure 3b. A clear impact of the nature of the TiO_2 support on the Mo oxidation states distribution is observed. As a matter of fact, Mo is more reduced on rutile (RNR) than on anatase (DT51D), the dominant states being Mo^{V} and Mo^{VI}, respectively. Mixed-phase P25 exhibits an intermediate Mo^{V}/Mo^{VI} ratio. Whereas the state of Mo on DT51D hardly changes, an overall oxidation of Mo occurs on RNR and P25 when switching from reduction to reaction conditions. This is ascribed to CO_2 and/or H_2O acting as oxidising agents,[56–58] and to the more labile oxygen environment of Mo on rutile than on

anatase due to higher reducibility of rutile than anatase.[59] Under reaction conditions, Mo/RNR is the only catalyst containing Mo^{IV} species. The latter may be at the origin of the significant methanol production activity exhibited by Mo/RNR (Fig. 2). However, the intermediate oxidation state of Mo/P25 with respect to DT51D and RNR counterparts does not correlate with an intermediate catalytic performance. Moreover, the NAP-XPS pressure conditions (2 mbar total pressure in all cases) are obviously not representative of those employed in the laboratory catalytic reactor (1 bar of H_2 for reduction, and 18 bar H_2 + 6 bar CO_2 for reaction). Thus, the measured Mo state differences between the supports should be considered qualitatively, and they are not sufficient to explain the catalytic data.

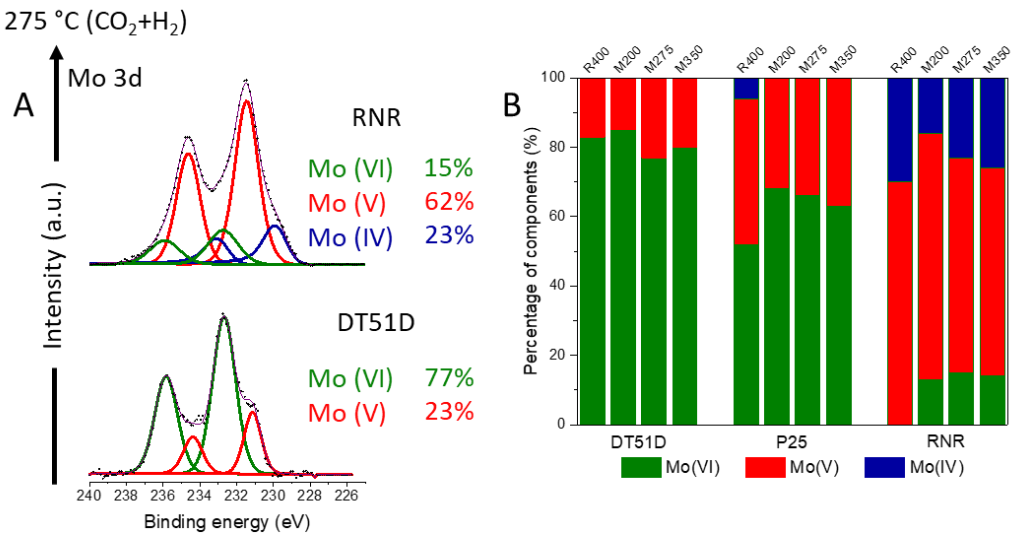

Figure 3 – A: Mo 3d NAP-XPS analysis at 275 °C under 2 mbar of a 3/1 H_2/CO_2 mixture on 3Mo/RNR (top) and 3Mo/DT51D (bottom). B: Mo oxidation state distribution in 3 wt% Mo supported on DT51D, P25 and RNR TiO_2 determined from NAP-XPS (Mo 3d), during in situ reduction at 400 °C (R400), and exposure to CO_2/H_2 reactant mixture (3/1) at 200 °C (M200), 275 °C (M275) and 350 °C (M350).

In order to gain insight into the reducibility of molybdenum on these three TiO_2 supports, H_2-TPR experiments were carried out, as shown in Figure 4. On the one hand, the amount of H_2 consumed per Mo atom increases with the fraction of rutile phase (i.e. from DT51D to RNR),

consistently with the NAP-XPS data showing the lowest overall oxidation state for Mo on RNR. On the other hand, the TPR peak position varies from 320 °C to 424 °C and 575 °C for RNR, DT51D and P25, respectively. This peak can be assigned to the reduction of well-dispersed octahedral Mo^{VI} species.[60–62] The last reduction event occurring above 800 °C can be attributed to tetrahedral Mo species[63] but is not relevant to our catalytic conditions.

While no significant H_2 consumption was observed for the bare supports, a continuous consumption occurs after the main reduction event, which can be explained by the slow reduction of polyoxomolybdate species.[62] The higher temperature necessary to reduce the Mo species on P25 is above the standard *in situ* reduction temperature used prior to our catalytic tests. This could be at the origin of the lower catalytic activity of this catalyst with respect to 3Mo/DT51D and 3Mo/RNR, in spite of the intermediate Mo oxidation state determined from NAP-XPS. Moreover, the higher reducibility of Mo on RNR could explain its superior catalytic performance.

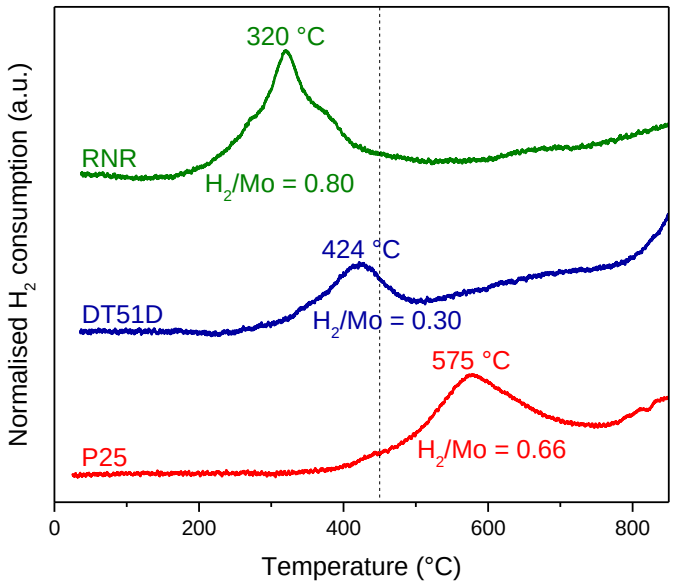

Figure 4 – H_2-TPR traces for 3 wt% Mo supported on RNR, DT51D and P25 titania. The temperatures of maximum consumption and the H_2-to-Mo molar ratios, i.e. area of the TPR peak normalised over the amount of Mo, are indicated. The temperature of in situ reduction pretreatment employed for catalytic tests (450 °C) is displayed with a vertical dotted line.

The effect of the *in situ* reduction temperature (450-700 °C) was investigated for 3Mo/DT51D. Figure S7 shows that the catalyst is already slightly active in the absence of *in situ* pretreatment. After *in situ* reduction at 450 °C, CO_2 conversion is much higher, and presents a maximum after treatment at 600 °C. However, the selectivity to methanol shows an opposite behaviour, i.e. a minimum for the R600 sample. The increase in conversion being superior to the decrease in selectivity, the methanol TOF (1.4 h^{-1}) is maximal after reduction at 600 °C. As shown by the STEM images in Figure S8, 3Mo/DT51D seems structurally stable at 450 °C, with no obvious effect of the *in situ* treatment. However, Mo sintering occurred for the R600 sample, as revealed by the presence of MoO_x nanoparticles of 2.0 ± 0.5 nm in size. A reducing treatment at 700 °C leads to even larger particles (2.7 ± 0.5 nm).

To discriminate the effect of *in situ* pre-reduction from that of Mo dispersion, a Mo/DT51D catalyst with a Mo loading as low as 0.3 wt% was tested after *in situ* reduction at 450 °C or 600

°C. Unlike for 3Mo/DT51D (Figure S7), the activity and methanol selectivity of 0.3Mo/DT51D both decrease when the reduction temperature increases. For the latter, the absence of nanoparticles demonstrated using STEM (Figure S9) suggests that the increase in conversion measured for 3Mo/DT51D-R600 is more related to the formation of nanoparticles than to a lower oxidation state. The low conversion obtained for 3Mo/DT51D-R700 is may be due to the excessive enlargement of Mo nanoparticles or/and a possible partial sintering of TiO_2 leading to a loss of specific surface area.[64]

Finally, the impact of the Mo loading (0.1-10 wt%) on the catalytic performance was investigated for Mo/DT51D-R450. The STEM images in Figure 5A show that Mo remains well-dispersed on titania even at high coverage, though Mo clusters (polyoxomolybdates) gradually replace single Mo atoms (monoxomolybdates) as the Mo coverage increases. Figure 5B shows an optimum in CO_2 conversion (5.2%) and methanol selectivity (10.2%) for 1 wt% Mo at 275 °C. This corresponds to a maximal methanol TOF of 3.6 h^{-1}.

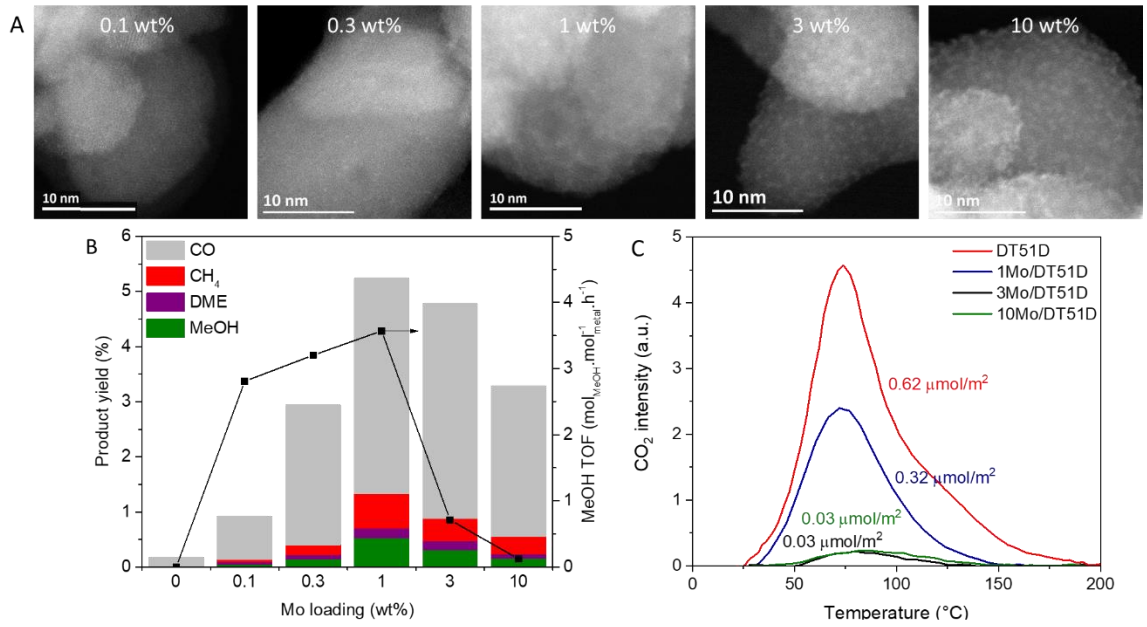

Figure 5 - A: Representative aberration-corrected STEM-HAADF micrographs of 0.1-10 wt% Mo/DT51D catalysts. B: Effect of Mo loading on CO/MeOH/CH_4/DME yields and methanol STY for 0-10 wt% Mo/DT51D-R450 at 275 °C under 30 bar of $H_2/CO_2/N_2$ (3/1/1), GHSV = 7500 mL.$g^{-1}.h^{-1}$. C: CO_2-TPD traces for 100 mg of 0-10 wt% Mo/DT51D samples. The total amount of desorbed CO_2 is indicated.

The decrease in CO_2 conversion below 1 wt% Mo is ascribed to a limiting number of active sites. However, the MeOH TOF remains nearly stable in the 0.1-1 wt% Mo loading range, which is assigned to the presence of mainly isolated oxomolybdate species on these three catalysts. The CO_2 TPD curves in Figure 5C show that the amount of CO_2 (adsorbed on the catalyst at RT and desorbed in the RT-450 °C range) decreases as the Mo loading increases, and vanishes to almost zero for 3 wt% Mo and above. We attribute the impact of Mo loading on the catalytic properties to a balance between the amount of basic sites on TiO_2 available for CO_2 adsorption and that of Mo centers enabling CO_2 conversion. A similar methanol activity tendency is observed for Mo/RNR with a MeOH TOF at 275 °C reaching 5.2 h^{-1} for the 1 wt% catalyst (Figure S10). Again, we ascribe this behaviour to the higher catalytic methanol production performance of isolated oxomolybdate species.

Conclusion

In conclusion, we have demonstrated the possibility to obtain efficient catalysts based on titania-supported ultradispersed molybdenum species for CO_2 hydrogenation to methanol. The TiO_2 support type, as well as the Mo loading and the reductive pretreatment temperature, substantially impact the catalytic activity and selectivity. In particular, a low Mo coverage corresponding to ca. 1 wt% Mo may provide an optimal compromise, in terms of methanol yield, between the number of active sites and their isolation. The active sites are probably associated to Mo isolated oxo species in partial oxidation states. The highest performance was measured for a titania support consisting of rutile nanorods, followed by commercial anatase. Forthcoming studies on the Mo/TiO_2 system will rely on advanced *operando* investigations and theoretical modelling. They will aim at understanding how the Mo atom coordination and oxidation state, as well as the titania surface structure and acid-base properties (including the presence of TiO_2 vacancies[65,66]) affect the catalytic properties. A better knowledge of the structure-function relationships will enable further improvement of the catalysts reported herein. This study represents a first step toward the development of new cost-efficient alternatives to Cu-Zn-based catalysts for CO_2 hydrogenation to methanol.

Acknowledgment

A. Nassereddine (IRCELYON) is acknowledged for preliminary catalysis experiments. Y. Lefkir & S. Reynaud (Laboratoire Hubert Curien) and M. Aouine (IRCELYON) are acknowledged for their support in STEM analysis. CLYM is acknowledged for access to the FEI Titan and Jeol NeoARM microscopes. N. Bonnet & P. Mascunan (IRCELYON) are acknowledged for XRF and BET analyses. Agence Nationale de la Recherche (UltraCat project, ANR-17-CE06-0008) is acknowledged for financial support. JL is a Serra Húnter Fellow and is grateful to the ICREA Academia program and projects MICINN/FEDER RTI2018-093996-B-C31 and GC 2017 SGR 128.

(1) Lu, X.-B.; Liang, B.; Zhang, Y.-J.; Tian, Y.-Z.; Wang, Y.-M.; Bai, C.-X.; Wang, H.; Zhang, R. Asymmetric Catalysis with CO2: Direct Synthesis of Optically Active Propylene Carbonate from Racemic Epoxides. *J. Am. Chem. Soc.* **2004**, *126* (12), 3732–3733. https://doi.org/10.1021/ja049734s.

(2) Ma, J.; Sun, N.; Zhang, X.; Zhao, N.; Xiao, F.; Wei, W.; Sun, Y. A Short Review of Catalysis for CO2 Conversion. *Catal. Today* **2009**, *148* (3), 221–231. https://doi.org/10.1016/j.cattod.2009.08.015.

(3) North, M.; Pasquale, R. Mechanism of Cyclic Carbonate Synthesis from Epoxides and CO2. *Angew. Chem. Int. Ed.* **2009**, *48* (16), 2946–2948. https://doi.org/10.1002/anie.200805451.

(4) Nie, X.; Li, W.; Jiang, X.; Guo, X.; Song, C. Recent Advances in Catalytic CO2 Hydrogenation to Alcohols and Hydrocarbons. *Adv. Catal.* **2019**, 121–233. https://doi.org/10.1016/bs.acat.2019.10.002.

(5) Saeidi, S.; Amin, N. A. S.; Rahimpour, M. R. Hydrogenation of CO2 to Value-Added Products—A Review and Potential Future Developments. *J. CO2 Util.* **2014**, *5*, 66–81. https://doi.org/10.1016/j.jcou.2013.12.005.

(6) Caparrós, F. J.; Soler, L.; Rossell, M. D.; Angurell, I.; Piccolo, L.; Rossell, O.; Llorca, J. Remarkable Carbon Dioxide Hydrogenation to Ethanol on a Palladium/Iron Oxide Single-Atom Catalyst. *ChemCatChem* **2018**, *10* (11), 2365–2369. https://doi.org/10.1002/cctc.201800362.

(7) Abou Hamdan, M.; Nassereddine, A.; Checa, R.; Jahjah, M.; Pinel, C.; Piccolo, L.; Perret, N. Supported Molybdenum Carbide and Nitride Catalysts for Carbon Dioxide Hydrogenation. *Front. Chem.* **2020**, *8*. https://doi.org/10.3389/fchem.2020.00452.

(8) Bowker, M. Methanol Synthesis from CO2 Hydrogenation. *ChemCatChem* **2019**, *11* (17), 4238–4246. https://doi.org/10.1002/cctc.201900401.

(9) Álvarez, A.; Bansode, A.; Urakawa, A.; Bavykina, A. V.; Wezendonk, T. A.; Makkee, M.; Gascon, J.; Kapteijn, F. Challenges in the Greener Production of Formates/Formic Acid, Methanol, and DME by Heterogeneously Catalyzed CO2 Hydrogenation Processes. *Chem. Rev.* **2017**, *117* (14), 9804–9838. https://doi.org/10.1021/acs.chemrev.6b00816.

(10) Alberico, E.; Nielsen, M. Towards a Methanol Economy Based on Homogeneous Catalysis: Methanol to H 2 and CO 2 to Methanol. *Chem. Commun.* **2015**, *51* (31), 6714–6725. https://doi.org/10.1039/C4CC09471A.

(11) Olah, G. A. Beyond Oil and Gas: The Methanol Economy. *Angew. Chem. Int. Ed.* **2005**, *44* (18), 2636–2639. https://doi.org/10.1002/anie.200462121.

(12) Huang, C.; Wen, J.; Sun, Y.; Zhang, M.; Bao, Y.; Zhang, Y.; Liang, L.; Fu, M.; Wu, J.; Ye, D.; Chen, L. CO2 Hydrogenation to Methanol over Cu/ZnO Plate Model Catalyst: Effects of Reducing Gas Induced Cu Nanoparticle Morphology. *Chem. Eng. J.* **2019**, *374*, 221–230. https://doi.org/10.1016/j.cej.2019.05.123.

(13) Carvalho, D. F.; Almeida, G. C.; Monteiro, R. S.; Mota, C. J. A. Hydrogenation of CO2 to Methanol and Dimethyl Ether over a Bifunctional Cu·ZnO Catalyst Impregnated on Modified γ-Alumina. *Energy Fuels* **2020**, *34* (6), 7269–7274. https://doi.org/10.1021/acs.energyfuels.0c00680.

(14) Wang, Z.; Song, H.; Pang, H.; Ning, Y.; Dao, T. D.; Wang, Z.; Chen, H.; Weng, Y.; Fu, Q.; Nagao, T.; Fang, Y.; Ye, J. Photo-Assisted Methanol Synthesis via CO2 Reduction under Ambient Pressure over Plasmonic Cu/ZnO Catalysts. *Appl. Catal. B Environ.* **2019**, *250*, 10–16. https://doi.org/10.1016/j.apcatb.2019.03.003.

(15) Yang, R.; Yu, X.; Zhang, Y.; Li, W.; Tsubaki, N. A New Method of Low-Temperature Methanol Synthesis on Cu/ZnO/Al2O3 Catalysts from CO/CO2/H2. *Fuel* **2008**, *87* (4–5), 443–450. https://doi.org/10.1016/j.fuel.2007.06.020.

(16) Behrens, M.; Studt, F.; Kasatkin, I.; Kühl, S.; Hävecker, M.; Abild-Pedersen, F.; Zander, S.; Girgsdies, F.; Kurr, P.; Kniep, B.-L.; Tovar, M.; Fischer, R. W.; Nørskov, J. K.; Schlögl, R. The Active Site of Methanol Synthesis over Cu/ZnO/Al2O3 Industrial Catalysts. *Science* **2012**, *336* (6083), 893–897. https://doi.org/10.1126/science.1219831.

(17) Kunkes, E. L.; Studt, F.; Abild-Pedersen, F.; Schlögl, R.; Behrens, M. Hydrogenation of CO2 to Methanol and CO on Cu/ZnO/Al2O3: Is There a Common Intermediate or Not? *J. Catal.* **2015**, *328*, 43–48. https://doi.org/10.1016/j.jcat.2014.12.016.

(18) Gaikwad, R.; Reymond, H.; Phongprueksathat, N.; Rohr, P. R. von; Urakawa, A. From CO or CO2?: Space-Resolved Insights into High-Pressure CO2 Hydrogenation to Methanol over Cu/ZnO/Al2O3. *Catal. Sci. Technol.* **2020**, *10* (9), 2763–2768. https://doi.org/10.1039/D0CY00050G.

(19) Element Scarcity - EuChemS Periodic Table. *EuChemS*.

(20) Liang, B.; Ma, J.; Su, X.; Yang, C.; Duan, H.; Zhou, H.; Deng, S.; Li, L.; Huang, Y. Investigation on Deactivation of Cu/ZnO/Al2O3 Catalyst for CO2 Hydrogenation to Methanol. *Ind. Eng. Chem. Res.* **2019**, *58* (21), 9030–9037. https://doi.org/10.1021/acs.iecr.9b01546.

(21) Martin, O.; Pérez-Ramírez, J. New and Revisited Insights into the Promotion of Methanol Synthesis Catalysts by CO 2. *Catal. Sci. Technol.* **2013**, *3* (12), 3343–3352. https://doi.org/10.1039/C3CY00573A.

(22) Zhong, J.; Yang, X.; Wu, Z.; Liang, B.; Huang, Y.; Zhang, T. State of the Art and Perspectives in Heterogeneous Catalysis of CO 2 Hydrogenation to Methanol. *Chem. Soc. Rev.* **2020**, *49* (5), 1385–1413. https://doi.org/10.1039/C9CS00614A.

(23) Ting, K. W.; Toyao, T.; Siddiki, S. M. A. H.; Shimizu, K. Low-Temperature Hydrogenation of CO2 to Methanol over Heterogeneous TiO2-Supported Re Catalysts. *ACS Catal.* **2019**, *9* (4), 3685–3693. https://doi.org/10.1021/acscatal.8b04821.

(24) Martin, O.; Martín, A. J.; Mondelli, C.; Mitchell, S.; Segawa, T. F.; Hauert, R.; Drouilly, C.; Curulla-Ferré, D.; Pérez-Ramírez, J. Indium Oxide as a Superior Catalyst for Methanol Synthesis by CO2 Hydrogenation. *Angew. Chem. Int. Ed.* **2016**, *55* (21), 6261–6265. https://doi.org/10.1002/anie.201600943.

(25) Frei, M. S.; Mondelli, C.; Short, M. I. M.; Pérez-Ramírez, J. Methanol as a Hydrogen Carrier: Kinetic and Thermodynamic Drivers for Its CO2-Based Synthesis and Reforming over Heterogeneous Catalysts. *ChemSusChem* **2020**, *n/a* (n/a). https://doi.org/10.1002/cssc.202001518.

(26) Piccolo, L. Restructuring Effects of the Chemical Environment in Metal Nanocatalysis and Single-Atom Catalysis. *Catal. Today* **2020**. https://doi.org/10.1016/j.cattod.2020.03.052.

(27) Zhang, H.; Liu, G.; Shi, L.; Ye, J. Single-Atom Catalysts: Emerging Multifunctional Materials in Heterogeneous Catalysis. *Adv. Energy Mater.* **2018**, *8* (1), 1701343. https://doi.org/10.1002/aenm.201701343.

(28) Wang, A.; Li, J.; Zhang, T. Heterogeneous Single-Atom Catalysis. *Nat. Rev. Chem.* **2018**, *2* (6), 65–81. https://doi.org/10.1038/s41570-018-0010-1.

(29) Mitchell, S.; Vorobyeva, E.; Pérez-Ramírez, J. The Multifaceted Reactivity of Single-Atom Heterogeneous Catalysts. *Angew. Chem. Int. Ed.* **2018**, *57* (47), 15316–15329. https://doi.org/https://doi.org/10.1002/anie.201806936.

(30) Liang, S.; Hao, C.; Shi, Y. The Power of Single-Atom Catalysis. *ChemCatChem* **2015**, *7* (17), 2559–2567. https://doi.org/10.1002/cctc.201500363.

(31) Dessal, C.; Sangnier, A.; Chizallet, C.; Dujardin, C.; Morfin, F.; Rousset, J.-L.; Aouine, M.; Bugnet, M.; Afanasiev, P.; Piccolo, L. Atmosphere-Dependent Stability and Mobility of Catalytic Pt Single Atoms and Clusters on γ-Al 2 O 3. *Nanoscale* **2019**, *11* (14), 6897–6904. https://doi.org/10.1039/C9NR01641D.

(32) Dessal, C.; Martínez, L.; Maheu, C.; Len, T.; Morfin, F.; Rousset, J. L.; Puzenat, E.; Afanasiev, P.; Aouine, M.; Soler, L.; Llorca, J.; Piccolo, L. Influence of Pt Particle Size and Reaction Phase on the Photocatalytic Performances of Ultradispersed Pt/TiO2 Catalysts for Hydrogen Evolution. *J. Catal.* **2019**, *375*, 155–163. https://doi.org/10.1016/j.jcat.2019.05.033.

(33) Dessal, C.; Len, T.; Morfin, F.; Rousset, J.-L.; Aouine, M.; Afanasiev, P.; Piccolo, L. Dynamics of Single Pt Atoms on Alumina during CO Oxidation Monitored by Operando X-Ray and Infrared Spectroscopies. *ACS Catal.* **2019**, *9* (6), 5752–5759. https://doi.org/10.1021/acscatal.9b00903.
(34) Zaman, S.; Smith, K. J. A Review of Molybdenum Catalysts for Synthesis Gas Conversion to Alcohols: Catalysts, Mechanisms and Kinetics. *Catal. Rev.* **2012**, *54* (1), 41–132. https://doi.org/10.1080/01614940.2012.627224.
(35) Wang, C.; Wang, D.; Liu, S.; Jiang, P.; Lin, Z.; Xu, P.; Yang, K.; Lu, J.; Tong, H.; Hu, L.; Zhang, W.; Chen, Q. Engineering the Coordination Environment Enables Molybdenum Single-Atom Catalyst for Efficient Oxygen Reduction Reaction. *J. Catal.* **2020**, *389*, 150–156. https://doi.org/10.1016/j.jcat.2020.05.034.
(36) Khan, M.; Xu, J.; Cao, W.; Liu, Z.-K. Mo-Doped TiO2 with Enhanced Visible Light Photocatalytic Activity: A Combined Experimental and Theoretical Study https://www-ingentaconnect-com.docelec.univ-lyon1.fr/content/asp/jnn/2014/00000014/00000009/art00051 (accessed Apr 8, 2020). https://doi.org/info:doi/10.1166/jnn.2014.8985.
(37) Chen, K.; Xie, S.; Bell, A. T.; Iglesia, E. Alkali Effects on Molybdenum Oxide Catalysts for the Oxidative Dehydrogenation of Propane. *J. Catal.* **2000**, *195* (2), 244–252. https://doi.org/10.1006/jcat.2000.3025.
(38) Faye, J.; Capron, M.; Takahashi, A.; Paul, S.; Katryniok, B.; Fujitani, T.; Dumeignil, F. Effect of Oxomolybdate Species Dispersion on Direct Methanol Oxidation to Dimethoxymethane over MoOx/TiO2 Catalysts. *Energy Sci. Eng.* **2015**, *3* (2), 115–125. https://doi.org/10.1002/ese3.53.
(39) Wang, D.; Qian, W.; Ishihara, A.; Kabe, T. Elucidation of Sulfidation State and Hydrodesulfurization Mechanism on Mo/TiO2 Catalyst Using 35S Radioisotope Tracer Methods. *Appl. Catal. Gen.* **2002**, *224* (1), 191–199. https://doi.org/10.1016/S0926-860X(01)00788-8.
(40) Ramirez, J.; Cedeño, L.; Busca, G. The Role of Titania Support in Mo-Based Hydrodesulfurization Catalysts. *J. Catal.* **1999**, *184* (1), 59–67. https://doi.org/10.1006/jcat.1999.2451.
(41) Ramirez, J.; Fuentes, S.; Díaz, G.; Vrinat, M.; Breysse, M.; Lacroix, M. Hydrodesulphurization Activity and Characterization of Sulphided Molybdenum and Cobalt—molybdenum Catalysts: Comparison of Alumina-, Silica-Alumina-and Titania-Supported Catalysts. *Appl. Catal.* **1989**, *52* (1), 211–224.
(42) Barrault, J.; Urresta, J. Hydrogénation du dioxyde de carbone en méthanol en présence de catalyseurs à base de molybdène. *Comptes Rendus Académie Sci. - Ser. IIC - Chem.* **1999**, *2* (3), 167–174. https://doi.org/10.1016/S1387-1609(99)80060-7.
(43) Kim, M. Y.; Ha, S. B.; Koh, D. J.; Byun, C.; Park, E. D. CO Methanation over Supported Mo Catalysts in the Presence of H2S. *Catal. Commun.* **2013**, *35*, 68–71. https://doi.org/10.1016/j.catcom.2013.02.004.
(44) Toyao, T.; Kayamori, S.; Maeno, Z.; Siddiki, S. M. A. H.; Shimizu, K. Heterogeneous Pt and MoOx Co-Loaded TiO2 Catalysts for Low-Temperature CO2 Hydrogenation To Form CH3OH. *ACS Catal.* **2019**, *9* (9), 8187–8196. https://doi.org/10.1021/acscatal.9b01225.
(45) Tougerti, A.; Berrier, E.; Mamede, A.-S.; La Fontaine, C.; Briois, V.; Joly, Y.; Payen, E.; Paul, J.-F.; Cristol, S. Synergy between XANES Spectroscopy and DFT to Elucidate the Amorphous Structure of Heterogeneous Catalysts: TiO2-Supported Molybdenum Oxide Catalysts. *Angew. Chem. Int. Ed.* **2013**, *52* (25), 6440–6444. https://doi.org/10.1002/anie.201300538.
(46) Hu, H.; Oliveira de Souza, D.; Berrier, E.; Paul, J.-F.; La Fontaine, C.; Briois, V.; Cristol, S.; Tougerti, A. Investigation of the Reducibility of Supported Oxomolybdate Species for Mapping of Active Centers of Partial Oxidation Reaction: In Situ Mo K-Edge XAS and DFT Study. *J. Phys. Chem. C* **2019**, *123* (30), 18325–18335. https://doi.org/10.1021/acs.jpcc.9b02732.
(47) Hu, H.; Wachs, I. E.; Bare, S. R. Surface Structures of Supported Molybdenum Oxide Catalysts: Characterization by Raman and Mo L3-Edge XANES https://pubs.acs.org/doi/pdf/10.1021/j100027a034 (accessed Jul 31, 2020). https://doi.org/10.1021/j100027a034.

(48) Domenichini, B.; Petukhov, M.; Rizzi, G. A.; Sambi, M.; Bourgeois, S.; Granozzi, G. Epitaxial Growth of Molybdenum on TiO2(110). *Surf. Sci.* **2003**, *544* (2), 135–146. https://doi.org/10.1016/j.susc.2003.07.013.
(49) Rizzi, G. A.; Reeder, A. E.; Agnoli, S.; Granozzi, G. Epitaxial MoOx Nanostructures on TiO2(110) Obtained Using Thermal Decomposition of Mo(CO)6. *Surf. Sci.* **2006**, *600* (16), 3345–3351. https://doi.org/10.1016/j.susc.2006.06.033.
(50) Krüger, P. Molybdenum Clusters on a TiO2(110) Substrate Studied by Density Functional Theory. *J. Phys. Chem. C* **2009**, *113* (13), 5308–5312. https://doi.org/10.1021/jp810886v.
(51) Nagai, M.; Kurakami, T. Reverse Water Gas Shift Reaction over Molybdenum Carbide. *J. Chem. Eng. Jpn.* **2005**, *38* (10), 807–812. https://doi.org/10.1252/jcej.38.807.
(52) Kharaji, A. G.; Shariati, A.; Takassi, M. A. A Novel γ-Alumina Supported Fe-Mo Bimetallic Catalyst for Reverse Water Gas Shift Reaction. *Chin. J. Chem. Eng.* **2013**, *21* (9), 1007–1014. https://doi.org/10.1016/S1004-9541(13)60573-X.
(53) Okemoto, A.; Harada, M. R.; Ishizaka, T.; Hiyoshi, N.; Sato, K. Catalytic Performance of MoO3/FAU Zeolite Catalysts Modified by Cu for Reverse Water Gas Shift Reaction. *Appl. Catal. Gen.* **2020**, *592*, 117415. https://doi.org/10.1016/j.apcata.2020.117415.
(54) Ma, Y.; Guo, Z.; Jiang, Q.; Wu, K.-H.; Gong, H.; Liu, Y. Molybdenum Carbide Clusters for Thermal Conversion of CO2 to CO via Reverse Water-Gas Shift Reaction. *J. Energy Chem.* **2020**, *50*, 37–43. https://doi.org/10.1016/j.jechem.2020.03.012.
(55) Ronda-Lloret, M.; Yang, L.; Hammerton, M.; Marakatti, V. S.; Tromp, M.; Sofer, Z.; Sepúlveda-Escribano, A.; Ramos-Fernandez, E. V.; Delgado, J. J.; Rothenberg, G.; Ramirez Reina, T.; Shiju, N. R. Molybdenum Oxide Supported on Ti3AlC2 Is an Active Reverse Water–Gas Shift Catalyst. *ACS Sustain. Chem. Eng.* **2021**, *9* (14), 4957–4966. https://doi.org/10.1021/acssuschemeng.0c07881.
(56) Zhang, L.; Wu, Z.; Nelson, N. C.; Sadow, A. D.; Slowing, I. I.; Overbury, S. H. Role Of CO2 As a Soft Oxidant For Dehydrogenation of Ethylbenzene to Styrene over a High-Surface-Area Ceria Catalyst. *ACS Catal.* **2015**, *5* (11), 6426–6435. https://doi.org/10.1021/acscatal.5b01519.
(57) Lee, T.; Jung, S.; Hong, J.; Wang, C.-H.; Alessi, D. S.; Lee, S. S.; Park, Y.-K.; Kwon, E. E. Using CO2 as an Oxidant in the Catalytic Pyrolysis of Peat Moss from the North Polar Region. *Environ. Sci. Technol.* **2020**, *54* (10), 6329–6343. https://doi.org/10.1021/acs.est.0c01862.
(58) Yao, R.; Herrera, J. E.; Chen, L.; Chin, Y.-H. C. Generalized Mechanistic Framework for Ethane Dehydrogenation and Oxidative Dehydrogenation on Molybdenum Oxide Catalysts. *ACS Catal.* **2020**, *10* (12), 6952–6968. https://doi.org/10.1021/acscatal.0c01073.
(59) Bouzoubaa, A.; Markovits, A.; Calatayud, M.; Minot, C. Comparison of the Reduction of Metal Oxide Surfaces: TiO2-Anatase, TiO2-Rutile and SnO2-Rutile. *Surf. Sci.* **2005**, *583* (1), 107–117. https://doi.org/10.1016/j.susc.2005.03.029.
(60) Arnoldy, P.; Jonge, J. C. M. D.; Moulijn, J. A. Temperature-programed reduction of molybdenum(VI) oxide and molybdenum(IV) oxide https://pubs.acs.org/doi/pdf/10.1021/j100267a021 (accessed Mar 19, 2021). https://doi.org/10.1021/j100267a021.
(61) Spojakina, A.; Kraleva, E.; Jiratova, K.; Petrov, L. TiO2-Supported Iron–molybdenum Hydrodesulfurization Catalysts. *Appl. Catal. Gen.* **2005**, *288* (1), 10–17. https://doi.org/10.1016/j.apcata.2005.02.034.
(62) Cedeño Caero, L.; Romero, A. R.; Ramirez, J. Niobium Sulfide as a Dopant for Mo/TiO2 Catalysts. *Catal. Today* **2003**, *78* (1), 513–518. https://doi.org/10.1016/S0920-5861(02)00342-5.
(63) Ghampson, I. T.; Pecchi, G.; Fierro, J. L. G.; Videla, A.; Escalona, N. Catalytic Hydrodeoxygenation of Anisole over Re-MoOx/TiO2 and Re-VOx/TiO2 Catalysts. *Appl. Catal. B Environ.* **2017**, *208*, 60–74. https://doi.org/10.1016/j.apcatb.2017.02.047.
(64) Quincy, R. B.; Houalla, M.; Proctor, A.; Hercules, D. M. Distribution of molybdenum oxidation states in reduced molybdenum/titania catalysts: correlation with benzene hydrogenation

activity https://pubs.acs.org/doi/pdf/10.1021/j100367a058 (accessed Apr 17, 2020). https://doi.org/10.1021/j100367a058.

(65) Ji, Y.; Luo, Y. New Mechanism for Photocatalytic Reduction of CO2 on the Anatase TiO2(101) Surface: The Essential Role of Oxygen Vacancy. *J. Am. Chem. Soc.* **2016**, *138* (49), 15896–15902. https://doi.org/10.1021/jacs.6b05695.

(66) Kattel, S.; Yan, B.; Chen, J. G.; Liu, P. CO2 Hydrogenation on Pt, Pt/SiO2 and Pt/TiO2: Importance of Synergy between Pt and Oxide Support. *J. Catal.* **2016**, *343*, 115–126. https://doi.org/10.1016/j.jcat.2015.12.019.